View Online / Journal Homepage / Table of Contents for this issue
Dynamic Article Links

Journal of Materials Chemistry

Cite this: J. Mater. Chem., 2012, 22, 6824

www.rsc.org/materials

PAPER

Forest-like TiO_2 hierarchical structures for efficient dye-sensitized solar cells†

Fang Shao, Jing Sun,* Lian Gao, Songwang Yang and Jianqiang Luo

Received 25th October 2011, Accepted 19th January 2012
DOI: 10.1039/c2jm15442k

Published on 27 February 2012 on http://pubs.rsc.org | doi:10.1039/C2JM15442K
Downloaded by University of Science and Technology of China on 18 October 2012

Forest-like TiO_2 hierarchical structures are prepared by the acid-assisted hydrothermal method without the use of any template or additive. The performances of dye sensitized solar cells (DSSCs) fabricated with the nanoforest structures are much higher than those assembled with nanorod array films. Crystalline nanorods and nanobranches act as preferential electron pathways for efficient charge collection. Nanobranches filling in the spaces among the nanorods increase the amount of dye-loading and enhance the light-harvesting property. Thus, our photoanode can take advantage of both fast electron transport and high surface area. DSSCs made of nanoforest films with a thin layer of nanocrystalline TiO_2 as the adhesive show the maximum energy conversion efficiency. Without any mediator, we can also fix films on FTO glasses through physical effects, which suggests potential applications in flexible solar cells.

1. Introduction

Dye-sensitized solar cells (DSSCs) are one of the most promising environmentally friendly energy-conversion devices.[1–3] To date, the most successful DSSCs were produced using porous nanoparticulate TiO_2 films. However, there are a lot of surface traps on the nanoparticles, resulting in serious charge recombination, which slows the electron transport rate and thus hinders progress in achieving higher performance.[4,5] It is believed that one-dimensional (1D) nanostructures can facilitate electron transport and reduce the charge recombination by providing a direct conduction pathway for the photogenerated electrons.[6–9] In particular, well aligned TiO_2 1D nanostructures grown perpendicular to the substrate are favored compared with random nanostructures. However, the insufficient surface area and the poor harvesting efficiency of simple 1D nanostructures constrain the energy conversion efficiency to relatively low levels.[10,11]

One way to solve this issue is to synthesize hierarchically structured photoanodes. In recent years, advanced hierarchical nanostructures, especially those with controllable morphologies at the three-dimensional (3D) nanosize level, have been synthesized and applied in DSSCs.[12–15] The control of the hierarchical structure at the nanosize level leads to novel and enhanced properties ranging from electrical to optical aspects. Development has followed a trend based on the need to improve photovoltaic efficiencies by increasing surface area. Among these, forest-like structures that consist of branched nanorod arrays, can offer greatly enhanced surface area while providing a direct pathway for the rapid collection of photogenerated electrons, therefore promising attractive potential applications in DSSCs. There have been some reports on the formation of branched 1D nanostructures. For example, Li *et al.*[16] reported the seeded heteroepitaxial selective growth of ZnO nanorods on TiO_2 nanorods and obtained the special dandelion-like ZnO–TiO_2 heterogeneous nanostructure. Ko *et al.*[17] prepared ZnO "nanoforest" photoanodes combining lengthwise growth and branched growth. The overall light-conversion efficiency of the branched ZnO nanowire DSSCs was 2.63%, which was much higher than that of upstanding ZnO nanowires. Zhang *et al.*[18] fabricated a delicate fishbone-like composite structure of titanate nanowire–anatase nanoshuttles by the self-sacrificing of titanate nanowires. However, despite the importance of forest-like TiO_2 photoanodes, little information is available on DSSCs based on branched TiO_2 nanorod arrays. Graetzel *et al.*[19] presented a DSSC fabricated with forest-like TiO_2 nanostructures assembly of nanoparticles. The structure was achieved by the expensive method of pulsed laser deposition and showed relatively low efficiency.

In this paper, we fabricated forest-like nanostructures *via* a low cost, solution processed hydrothermal method. The nanobranches with good connections to the trunk are single-crystals. Such structures that combine the properties of 3D and 1D nanostructures may be a more interesting alternative than simple arrays of nanorods due to their higher specific surface area and porosity, especially for application in DSSCs.[20] Using the obtained forest-like TiO_2 nanostructures as photoanodes in DSSCs can significantly increase the power conversion efficiency.

The State Key Lab of High Performance Ceramics and Superfine Microstructure, Shanghai Institute of Ceramics, Chinese Academy of Sciences, 1295 Ding Xi Road, Shanghai, 200050, China. E-mail: jingsun@mail.sic.ac.cn; Fax: +86 21 52414301; Tel: +86 21 52413903

† Electronic Supplementary Information (ESI) available: SEM images of the films without H_2SO_4 treatment, high resolution SEM image of the nanoforest films obtained by H_2SO_4 hydrothermal treatment or H_2SO_4 corrosion on the heating holder, SEM images of TiO_2 on FTO glasses and photographic images of the NT2 photoanodes. See DOI: 10.1039/c2jm15442k

This journal is © The Royal Society of Chemistry 2012

Published on 27 February 2012 on http://pubs.rsc.org | doi:10.1039/C2JM15442K
Downloaded by University of Science and Technology of China on 18 October 2012

The efficiency increase can be attributed to the increased surface area, enabling higher dye loading and light harvesting while providing direct conductive pathways for charge transfer along the crystalline TiO_2 nanorods and nanobranches.

We fixed TiO_2 films onto FTO glasses *via* two methods for front-illuminated DSSCs. First, we transferred the films using a thin layer of TiO_2 nanocrystal paste. With this method, the obtained DSSCs have good performances but the paste has to be calcinated at high temperature. Here, we report another method to adhere the films on FTO glasses without any mediator. The obtained DSSCs have longer electron life but less dye loading and poorer efficiency. Given that the films are fixed on FTO glasses through physical effects, this method may be applicable to flexible DSSCs.

2. Experimental

2.1 Nanorod and nanotree array synthesis

The $H_2Ti_2O_5 \cdot H_2O$ nanorods were prepared according to our previous work.[21] After cleaning the titanium plates (99.97% purity, 0.25 mm thickness, Sigma-Aldrich) with distilled water, ethanol and acetone, $Na_2Ti_2O_5 \cdot H_2O$ nanorods were grown on the plates *via* a hydrothermal treatment with aqueous NaOH. The reaction time was 24 h and the temperature was kept at 220 °C. After cooling down to room temperature, the obtained $Na_2Ti_2O_5 \cdot H_2O$ covered titanium plates were washed with deionized water and ethanol several times, and dried at 60 °C for 10 min. Then, the $H_2Ti_2O_5 \cdot H_2O$ films on titanium plates were obtained by subsequently immersing the samples in dilute HCl to exchange the Na^+ with H^+.

The as-prepared $H_2Ti_2O_5 \cdot H_2O$ films were transferred to autoclaves with 25 mL 0.02 M H_2SO_4 aqueous solution. The autoclaves were kept in an electric oven at 100 °C for 4 h. Then, the nanotree array films were successfully synthesized. In order to investigate the formation mechanism of the hierarchical architectures, some experiments were carried out with different preparation conditions.

2.2 Photoanodes and DSSC fabrication

Two methods were employed to prepare TiO_2 photoanodes. **Method 1:** The as-prepared nanorod and nanotree arrays were detached from the Ti plates, and transferred onto the FTO substrate with a layer of nanocrystalline TiO_2 paste as an adhesive. Then, the attached films were annealed at 500 °C for 30 min in air. The obtained TiO_2 nanorods and nanotrees were labeled as NR1 and NT1, respectively. **Method 2:** Immerse the as-prepared films and FTO glasses in deionized water, and drag the films onto glasses using tweezers. Then, use a straw to remove the excessive water. When dried, the films were adhered onto the glasses. Finally, the samples were also calcined at 500 °C and the samples were denoted as NR2 and NT2 correspondingly.

Upon cooling down to 80 °C, the various TiO_2 films were immersed in a solution containing 0.3 mM N719 dye in a mixture of 1 : 1 acetonitrile–tert-butyl alcohol for 24 h. These sensitized photoanodes and the Pt-FTO counter electrode were assembled as a sandwich-type cell and separated by a polymer foil. A drop of the electrolyte which contained 0.5 M LiI, 0.05 M I_2 and 0.5 M tert-butylpyridine in acetonitrile was introduced between the two electrodes.

2.3 Characterization

Structural characterization of the synthesized films was done using a powder X-ray diffraction (XRD, D/max 2550V, Rigaku Tokyo, Japan). The morphology was obtained by field emission scanning electron microscopy (FESEM, JSM-6700F, JEOL Tokyo, Japan) and the details of the structure were determined with transmission electron microscopy (TEM/HRTEM, JEM-200CX, JEOL Tokyo, Japan), along with selected area electron diffraction (SAED) patterns. Reflectance and absorption spectra were obtained by a UV-Vis spectrometer (Lambda 950, Perkin-Elmer, Waltham, MA). The photocurrent–voltage of the DSSCs was measured on an electrochemical workstation (Model CHI 660C, CH) with an AM 1.5 solar simulator (100 mW cm^{-2}, Model YSS-80A, Yamashita). The active area of photoanodes was 0.12 cm^2, determined by an aperture mask. Differences in dye uptake were measured through the optical absorption spectra of the resulting solution obtained after soaking the films in 0.1 M NaOH aqueous solution. The incident photon-to-current conversion efficiency (IPCE) was measured using a 300 W Xe lamp as a light source and the data were collected at AC mode. Electrochemical impedance spectroscopy (EIS) curves of the DSSCs were also observed. The frequency range was varied from 0.1 Hz to 100 kHz. The applied bias voltage was set to the open-circuit voltage (V_{OC}) of the DSSC, which had been determined earlier.

3. Results and discussion

Typical XRD patterns of various films are illustrated in Fig. 1. In our earlier work, $H_2Ti_2O_5 \cdot H_2O$ nanorod films were prepared by the hydrothermal method, the XRD pattern of which is shown in Fig. 1a. After H_2SO_4 corrosion, the crystal phase changed greatly. The diffraction peaks from anatase, rutile and the parent $H_2Ti_2O_5 \cdot H_2O$ can be observed in the reaction product (Fig. 1b). Sharp diffraction peaks imply that the as-prepared TiO_2 is crystalline. As shown in Fig. 1c, after being calcinated at 500 °C

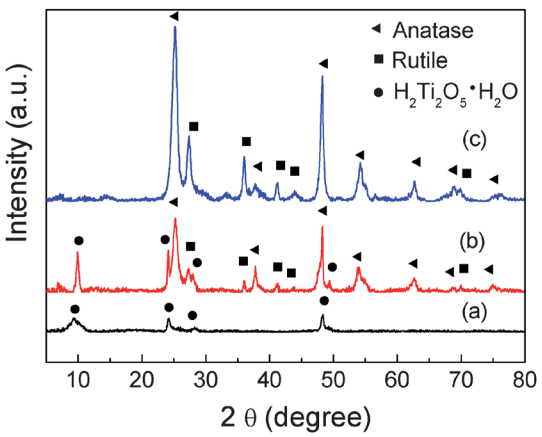

Fig. 1 XRD patterns of various films (a) before H_2SO_4 treatment, (b) after H_2SO_4 treatment, (c) after being calcinated at 500 °C for 30 min.

Downloaded by University of Science and Technology of China on 18 October 2012
Published on 27 February 2012 on http://pubs.rsc.org | doi:10.1039/C2JM15442K

for 30 min, the $H_2Ti_2O_5 \cdot H_2O$ phase disappears while the peak intensities of anatase and rutile are both enhanced.

SEM images of the $H_2Ti_2O_5 \cdot H_2O$ nanorod arrays without H_2SO_4 treatment are shown in Fig. S1 (ESI†). The distinct rod morphology can be observed with smooth and clean surfaces. The diameters of the nanorods are 50–150 nm and the lengths are over 10 μm. Fig. 2a,b exhibits the morphology of the films treated by an acid-assisted hydrothermal process at 100 °C for 4 h. It can be found that the rod morphology changed to a tree-like branched nanorod structure with branches of about 150 nm. The length and diameter of the nanorods both decrease, to around 7.0 μm and 40 nm, respectively. The SEM image at higher resolution (Fig. S2, ESI†) indicates that there is a layer of nanoparticles closely coated on the surface of the nanorods. As shown in Fig. 2c,d, heat treatment at 500 °C for 30 min does not destroy the nanoforest morphology. However, the calcination makes the two structures combine closely together.[22]

To better understand the structure and the contact state of the TiO_2 hierarchical structures, TEM/HRTEM measurements were taken to study the sample after hydrothermal corrosion and heat treatment. Fig. 3a shows the low-magnification TEM image of a part of the TiO_2 nanotree structure. The surface of the nanorods appears to be very coarse, and many nanoparticles and nanobranches are observed on the surface. The nanobranches are not growing perpendicular to the nanorod surface but at an angle. Besides, the nanobranch is found to anchor to the nanorod effectively with large-area connection. The nanobranch can be indexed to anatase with a [001] growth direction (Fig. 3b). As shown, there is no obvious interface between the nanobranch and the nanorod. The crystal lattice of the nanobranch is continuous with that of the nanorods and the lattice mismatch between the two structures is small, so there are few defects at grain boundaries as trapping sites, which favors charge migration.[16] Fig. 3c–e are SAED patterns recorded by focusing specifically at the nanobranch, nanorod and the junction regions respectively. The images indicate that the nanobranch is single-crystalline with good crystallinity.

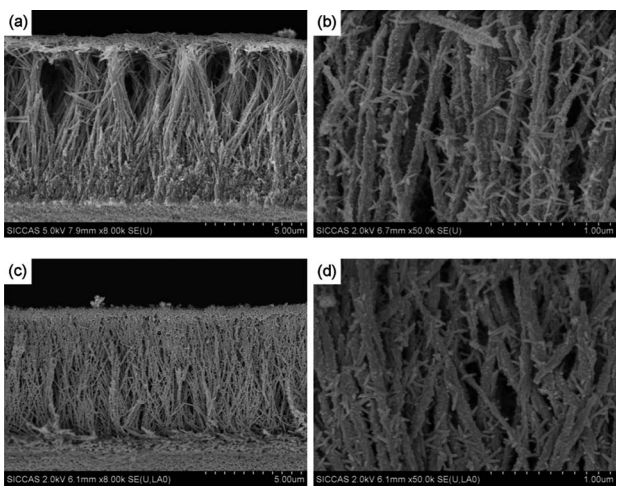

Fig. 2 Top view and cross-sectional view of the obtained films. (a), (b) the films after H_2SO_4 hydrothermal corrosion, (c), (d) the films after being calcinated at 500 °C for 30 min.

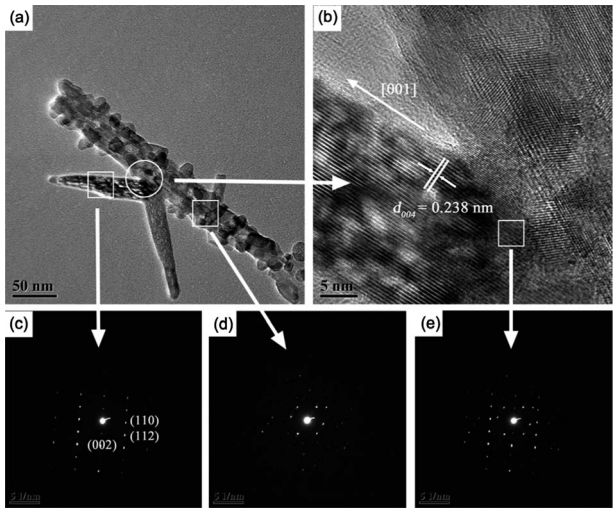

Fig. 3 (a) TEM image of a part of the TiO_2 nanotree structure, (b) the corresponding HRTEM image of the boundary for the structure, (c–e) the corresponding SAED patterns for the nanobranch, nanorod and boundary.

In order to investigate the formation mechanism of the hierarchical architectures, some other experiments were carried out with different formation conditions. First, we extended the hydrothermal corrosion time to 6 h and found that the films were destroyed, becoming dispersed powders. Secondly, we used ordinary heating instead of hydrothermal action to corrode the as-prepared $H_2Ti_2O_5 \cdot H_2O$ films as follows. The $H_2Ti_2O_5 \cdot H_2O$ films were transferred to a Petri dish with 25 mL 0.02 M H_2SO_4 aqueous solution. The Petri dish was then put on a heating holder and kept at 100 °C for 4 h. Through this process, we can still get the nanoforest structures (Fig. 4). From the SEM images at higher resolution in Fig. S3 (ESI†), it can be seen that the diameter of a typical nanorod is about 89 nm and the length is 8.5 μm, approximately. The nanobranches are clearly smaller and fewer in number than those prepared by the hydrothermal process while the nanorods are bigger. The results reveal that the $H_2Ti_2O_5 \cdot H_2O$ nanorods are consumed gradually with the formation of nanobranches, indicating that the transformation mechanism is the dissolution–recrystallization mechanism.

On the basis of the above experimental facts and some previous reports,[18,22,23] a possible mechanism has been proposed for the transformation from nanorod to nanotree arrays in the hydrothermal process. The formation process of the forest-like hierarchical structures is shown in Scheme 1. First, the $H_2Ti_2O_5 \cdot H_2O$ nanorods react with the H_2SO_4 as follows:

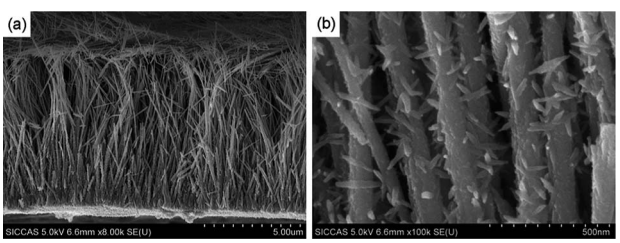

Fig. 4 SEM images of the nanoforest structures obtained by heating on the heating holder instead of hydrothermal reaction.

This journal is © The Royal Society of Chemistry 2012

Published on 27 February 2012 on http://pubs.rsc.org | doi:10.1039/C2JM15442K
Downloaded by University of Science and Technology of China on 18 October 2012

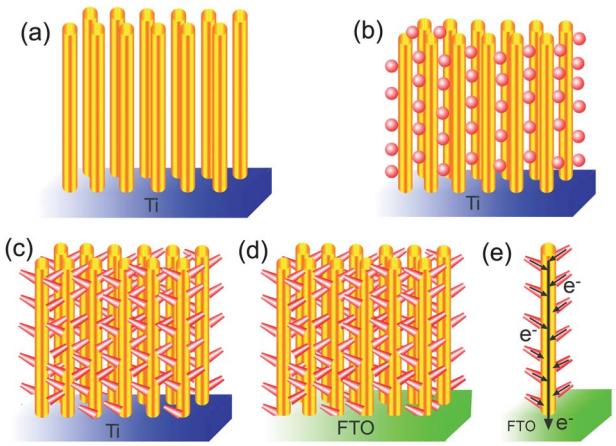

Scheme 1 (a)–(d) Schematic procedure for the formation of the forest-like hierarchical photoanodes. (e) A cartoon of the presumed preferential electron pathway in the hierarchical photoanodes.

$$H_2SO_4 + H_2Ti_2O_5 \cdot H_2O \rightarrow Ti(SO_4)_2 + H_2O \quad (1)$$

Then the TiO_2 nanoparticles are deposited on the surface of the $H_2Ti_2O_5 \cdot H_2O$ nanorods by the hydrolysis of $Ti(SO_4)_2$:

$$Ti(SO_4)_2 + H_2O \rightarrow TiO_2 + H_2SO_4 \quad (2)$$

The surface of the nanorods plays an important role in the process by providing a Ti source and locations for the deposition. The initial nanoparticles are gradually transformed into dendritic crystals with increasing reaction time, and finally into monocrystals. During the process, the smaller particles disappear while the larger ones grow, just like Ostwald ripening. Finally, forest-like TiO_2 hierarchical structures are formed by calcining the TiO_2–$H_2Ti_2O_5 \cdot H_2O$ films. The film geometry and the crystalline nature provide a large surface area and allow a fast and efficient transfer of the photo-generated electrons from the dye molecule to the FTO substrate, as shown in Scheme 1e, leading to reduced electron–hole recombination and improved photocurrent and efficiency.[24] This hierarchical structure can also avoid forming a large amount of grain boundaries, since the nanobranches grow on nanorods by self-sacrificing of the nanorods.

Four different TiO_2 photoanodes were prepared using two methods. SEM images of various TiO_2 films on FTO substrates are shown in Fig. S4 (ESI†), from which we can clearly see the differences of the four photoanodes. After transferral to the FTO glasses, all of the films maintained the morphologies of nanorod or nanotree arrays. What's more, the connection between the films and FTO glasses appears good though the sample preparation may have a negative effect on the structure.

Fig. 5 shows the reflectance spectra of the four different TiO_2 photoanodes. The measured reflectances of TiO_2 nanotree films were found to be remarkably higher than those of TiO_2 nanorod films. The better reflection was due to the interwoven nanobranches, which can effectively confine the incident light in electrodes, thus improving the light-harvesting efficiency. Without the TiO_2 nanoparticle paste, the reflection of nanorod and nanotree films are both reduced, this can be explained by the decrease of the whole TiO_2 amount in photoanodes.

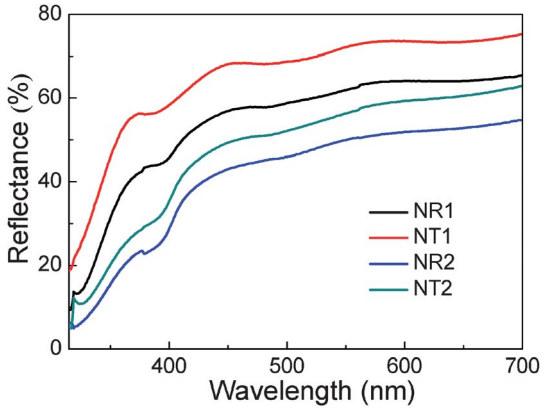

Fig. 5 Reflectance spectra of the four different TiO_2 photoanodes.

DSSC sandwich type cells were constructed with the sensitized TiO_2 photoanodes and their performances were evaluated by recording current–voltage (J–V) characteristics under normalized illumination (Fig. 6). All of the detailed values are shown in Table 1. For the NR1 based solar cell the generated photocurrent (J_{SC}) is 8.72 mA cm^{-2} while the J_{SC} is 10.90 mA cm^{-2} for the NT1 based solar cell. The open-circuit photovoltage (V_{OC}) and the fill factor (FF) of the two cells are almost the same, about 0.71 V and 69.82%, respectively. The overall light conversion efficiency (η) increases from 4.34% (NR1 cell) to 5.45% (NT1 cell). We can see that by implementing additional branches, the J_{SC} and η could be significantly increased due to the increased effective surface area and the enhanced light-harvesting property by scattering enhancement and trapping without sacrificing efficient electron transport. In contrast, nanorod arrays are not favorable for light harvesting because photons could possibly travel between the vertical nanorods without being absorbed by the dye.[25] The dye-immersed photoanodes were soaked in a 0.1 M NaOH aqueous solution to desorb the dye. The amount of desorbed dye was quantified by measuring the optical absorption spectra. The amount of dye loading in NT1 was found to be 2.37 $\times$ 10^{-8} mol cm^{-2}, higher than the value of 1.70 $\times$ 10^{-8} mol cm^{-2} corresponding to the dyed NR1 photoanode. The augmented surface area results in increased dye loading.

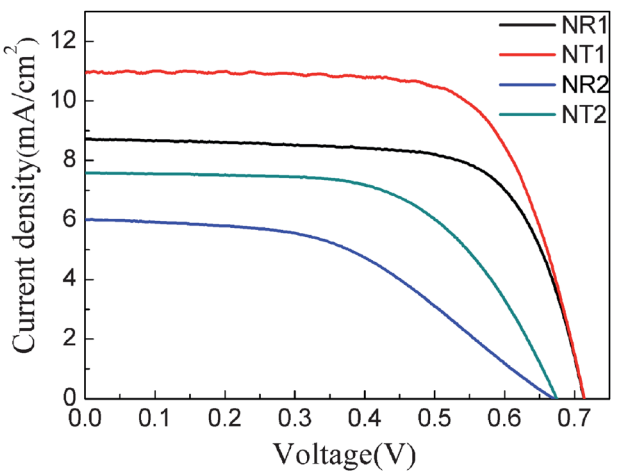

Fig. 6 J–V characteristics of dye-sensitized solar cells assembled with different TiO_2 photoanodes.

Table 1 Performance characteristics of DSSCs based on various photoanodes

Photoanodes	V_{OC}/V	J_{SC}/mA cm^{-2}	FF (%)	η (%)	Amount of dye/ 10^{-8} mol cm^{-2}
NR1	0.71	8.72	69.82	4.34	1.70
NT1	0.71	10.90	69.81	5.45	2.37
NR2	0.67	6.02	46.92	1.89	0.61
NT2	0.67	7.58	59.85	3.06	0.96

Downloaded by University of Science and Technology of China on 18 October 2012
Published on 27 February 2012 on http://pubs.rsc.org | doi:10.1039/C2JM15442K

Furthermore, we can still get photoanodes without any mediators. As shown in Fig. S5 (ESI†), the TiO_2 film is almost as large as the FTO substrate, and it shows no curling, cracking or collapse. Compared with NR1 and NT1, the absorbed dye in NR2 and NT2 are reduced enormously. Along with the decreased dye due to the lack of the TiO_2 nanoparticles layer, there is another reason that may dramatically influence the dye loading. As shown in Fig. S5b and c (ESI†), the colors of the front and back of the sensitized photoanodes are different. The back side exhibits a kind of pale color, indicating insufficient dye absorption. The bottoms of the nanorod and nanotree structures are compacted, as demonstrated in the SEM images. For NR2 and NT2, the bottom of the films are adhered closely to the FTO glasses, therefore the dye can hardly infiltrate to the bottom part. However, for NR1 and NT1, dye can easily sensitize the bottom through the porous nanoparticles. So, the performances of DSSCs with NR2 and NT2 are relatively poor. The efficiency of the TiO_2 nanorods directly adhered on FTO (NR2) was only 1.89%. After H_2SO_4 treatment, the V_{OC} shows no change while the J_{SC} is enhanced from 6.02 to 7.58 mA cm^{-2}. It's worth noting that unlike NR1 and NT1, the FF of NT2 is much bigger than that of NR2. It indicates that the H_2SO_4 treatment may lead to inhibited recombination and efficient carrier collection from the TiO_2 films to FTO glasses.[26] The DSSC based on NT2 yields a power conversion efficiency of 3.06%, 61.90% higher than that of NR2.

The UV-vis spectra of dye sensitized films (on FTO glasses) are shown in Fig. 7. Compared with sensitized nanorod arrays, the nanoforest film shows an enhanced response over a wide spectral range, even up to long wavelengths (>600 nm), where the dye absorbs weakly. Besides, the samples prepared by method 1 have a much higher absorption than those obtained with method 2. The increase of absorption magnitude can be attributed to the enhanced dye adsorption and light scattering caused by the modification or the presence of TiO_2 nanoparticles. The inconspicuous dye absorption peaks and the high absorption in low wavelength ranges may result from the intrinsic optical absorption of TiO_2 and the reflection of the TiO_2 films.

Fig. 8 exhibits the IPCE data collected under AC mode, the trends are in good agreement with the other test results. The morphology and surface area of the photoanode film have enormous influence on the IPCE. Nanoforests had higher IPCE values over the whole wavelength range than nanorod arrays. Method 1 also helped to significantly improve the results. The increase was consistent with the increase of J_{SC} shown in Fig. 6. The enhanced IPCE and photocurrent are likely to be related to the change of absorption characteristics as observed in UV-vis spectra in Fig. 7. Comparing Fig. 7 with Fig. 8, it can be found that the trends for different samples are consistent. But the dye absorption peaks in Fig.7 are not as obvious as those in Fig.8. This can be ascribed to the influence of the reflection and the intrinsic optical absorption of TiO_2.

To gain better insight into the dynamics of charge transfer processes, electrochemical impedance spectroscopy (EIS) measurements under AM1.5G, 1 sun illumination were conducted at the open circuit voltage of the cells. The spectra are displayed in Fig. 9. As reported in other works,[27–29] the three semicircles that appeared in order of decreasing frequency in Nyquist diagrams are classically assigned to the charge-transfer resistance at the interface of the counter electrode–electrolyte (R_{pt}), the charge-transfer resistance occurring at the TiO_2–dye–electrolyte interface (R_{ct}) and the Nernst diffusion in the electrolyte. As shown, in the cases of NR1 and NT1, the size of the semicircle at mid-range frequency becomes much smaller after

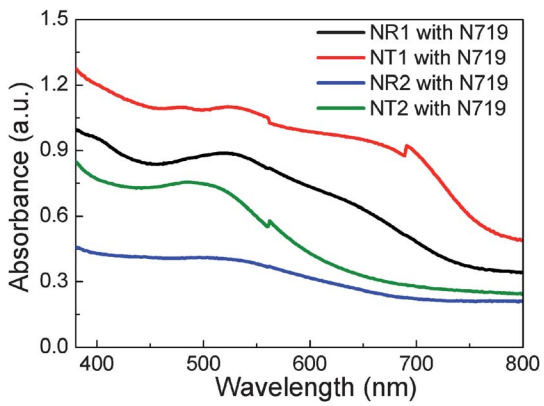

Fig. 7 UV-vis absorption spectra of the four sensitized TiO_2 photoanodes.

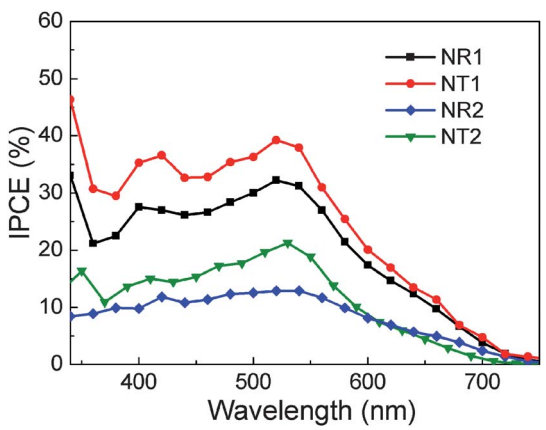

Fig. 8 IPCE curves of DSSCs based on NR1, NT1, NR2 and NT2.

This journal is © The Royal Society of Chemistry 2012

Downloaded by University of Science and Technology of China on 18 October 2012
Published on 27 February 2012 on http://pubs.rsc.org | doi:10.1039/C2JM15442K

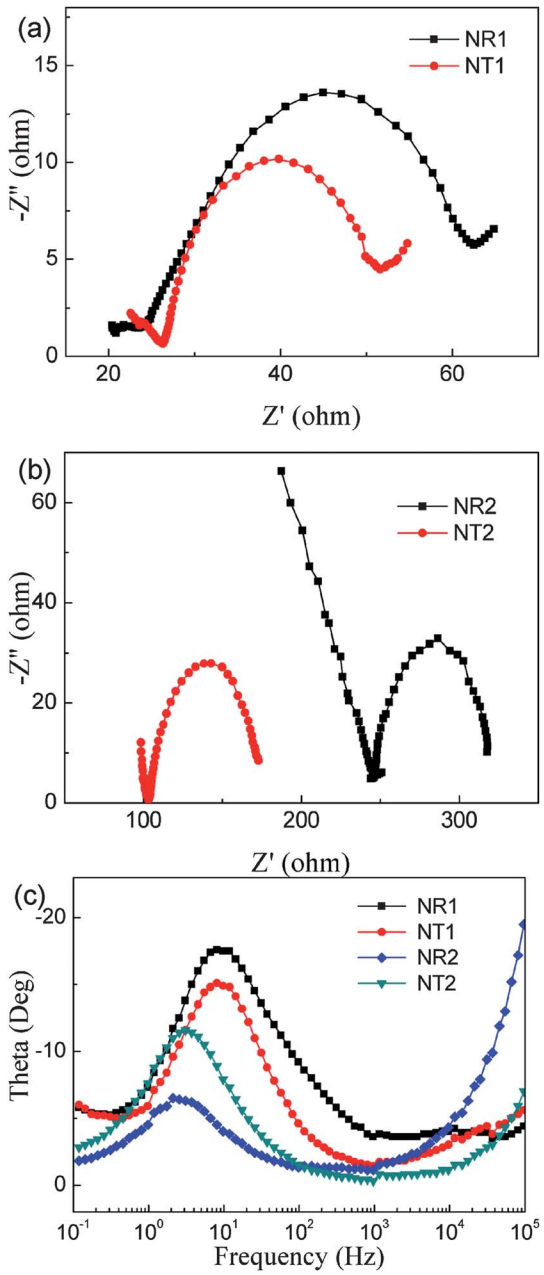

Fig. 9 Electrochemical impedance spectra of the TiO_2 nanostructures. (a) Nyquist plots of NR1 and NT1, (b) Nyquist plots of NR2 and NT2, (c) Bode plots.

the H_2SO_4 treatment. It indicates that the TiO_2 photoanodes with a nanoforest structure can provide much lower charge-transfer resistance than nanorods, which could be an important factor for the improvement of the performance of the DSSCs with nanoforest structures. The resistances of NR2 and NT2 are much larger than those of NR1 and NT1, suggesting that the electron extraction from nanoparticles to the FTO substrate is better than that from nanorods or nanotrees to the FTO glass due to the better connection.[30] For NT2, the characteristic semicircles shift a lot to smaller resistance compared with the NR2 electrode, confirming the better connection at the nanoforest TiO_2–FTO interface. Fig. 9c illustrates the Bode plots of the DSSCs fabricated with the four different electrodes. The mid-range frequency peaks (1–10 Hz) of the electrodes can be observed from the plots and the electron lifetime (τ_n) in photoanodes can be related to the inverse of frequency (f_{mid}) as in eqn (3).[31–33]

$$\tau_n = 1/2\pi f_{mid} \quad (3)$$

For NR2 and NT2, the values of τ_n are about 75.65 ms and 51.53 ms, which are significantly higher compared with 19.73 ms for the NR1 and NT1 electrodes. The results reveal that the existence of an interface, created by the TiO_2 nanoparticle paste used to fix the TiO_2 arrays onto FTO, might result in charge recombination during the electron transfer between nanoparticles.[34]

4. Conclusions

Forest-like TiO_2 hierarchical nanostructures are synthesized by a low cost, solution processed method, and photoanodes made of the nanoforest films are proposed for dye sensitized solar cells. The experimental results show that the above-mentioned photoanode can noticeably improve the performance of the solar cell. Two methods were adopted to fabricate photoanodes, with or without TiO_2 nanoparticle paste. Under the same fabrication conditions, the solar cells made with the nanoforest films demonstrated 25.58% and 61.90% higher efficiency than those made using nanorod array films. The efficiency increase is due to the greatly enhanced surface area for higher dye loading and light harvesting, and also due to the reduced charge recombination by providing direct conduction pathways along the nanorods and branches. The DSSCs with TiO_2 nanoparticle paste have better performance. However, using physical effects to fix the films on FTO glasses can increase the electron life, and it may be compatible with lightweight flexible plastic and other fragile substrates.

Acknowledgements

This work was supported by the National Natural Science Foundation of China (Grant No. 50972157).

References

1 B. Oregan and M. Gratzel, *Nature*, 1991, **353**, 737–740.
2 M. Durr, A. Schmid, M. Obermaier, S. Rosselli, A. Yasuda and G. Nelles, *Nat. Mater.*, 2005, **4**, 607–611.
3 Y. J. Kim, M. H. Lee, H. J. Kim, G. Lim, Y. S. Choi, N. G. Park, K. Kim and W. I. Lee, *Adv. Mater.*, 2009, **21**, 3668–3673.
4 S. H. Kang, S. H. Choi, M. S. Kang, J. Y. Kim, H. S. Kim, T. Hyeon and Y. E. Sung, *Adv. Mater.*, 2008, **20**, 54–58.
5 K. Zhu, N. R. Neale, A. Miedaner and A. J. Frank, *Nano Lett.*, 2007, **7**, 69–74.
6 M. Law, L. E. Greene, J. C. Johnson, R. Saykally and P. D. Yang, *Nat. Mater.*, 2005, **4**, 455–459.
7 C. A. Grimes, G. K. Mor, O. K. Varghese, M. Paulose and K. Shankar, *Sol. Energy Mater. Sol. Cells*, 2006, **90**, 2011–2075.
8 H. E. Wang, Z. H. Chen, Y. H. Leung, C. Y. Luan, C. P. Liu, Y. B. Tang, C. Yan, W. J. Zhang, J. A. Zapien, I. Bello and S. T. Lee, *Appl. Phys. Lett.*, 2010, **96**, 263104.
9 B. Liu, J. E. Boercker and E. S. Aydil, *Nanotechnology*, 2008, **19**, 505604.
10 B. Liu and E. S. Aydil, *J. Am. Chem. Soc.*, 2009, **131**, 3985–3990.
11 C. K. Xu, P. H. Shin, L. L. Cao, J. M. Wu and D. Gao, *Chem. Mater.*, 2010, **22**, 143–148.

View Online

12 W. G. Yang, F. R. Wan, Y. L. Wang and C. H. Jiang, *Appl. Phys. Lett.*, 2009, **95**, 133121.
13 F. Xu, M. Dai, Y. N. Lu and L. T. Sun, *J. Phys. Chem. C*, 2010, **114**, 2776–2782.
14 C. Y. Jiang, X. W. Sun, G. Q. Lo, D. L. Kwong and J. X. Wang, *Appl. Phys. Lett.*, 2007, **90**, 263501.
15 J. K. Oh, J. K. Lee, H. S. Kim, S. B. Han and K. W. Park, *Chem. Mater.*, 2010, **22**, 1114–1118.
16 C. Z. Li, F. Gu, L. L. Gai, W. Shao and L. Schmidt-Mende, *Chem. Commun.*, 2011, **47**, 8400–8402.
17 S. H. Ko, D. Lee, H. W. Kang, K. H. Nam, J. Y. Yeo, S. J. Hong, C. P. Grigoropoulos and H. J. Sung, *Nano Lett.*, 2011, **11**, 666–671.
18 L. Zhang, H. K. Wang, W. Shao, F. Gu, M. K. Lu and C. Z. Li, *Inorg. Chem.*, 2009, **48**, 9732–9736.
19 F. Di Fonzo, F. Sauvage, A. L. Bassi, C. S. Casari, V. Russo, G. Divitini, C. Ducati, C. E. Bottani, P. Comte and M. Graetzel, *Nano Lett.*, 2010, **10**, 2562–2567.
20 Z. J. Chang, *Chem. Commun.*, 2011, **47**, 4427–4429.
21 F. Shao, J. Sun, L. Gao, S. W. Yang and J. Q. Luo, *J. Phys. Chem. C*, 2011, **115**, 1819–1823.
22 H. Liu, W. J. Zhou, G. J. Du, P. G. Hu, G. H. Li, D. Z. Wang, J. Y. Wang, R. I. Boughton, D. Liu and H. D. Jiang, *J. Mater. Chem.*, 2011, **21**, 7937–7945.
23 H. Y. Zhu, X. P. Gao, Y. Lan, D. Y. Song, Y. X. Xi and J. C. Zhao, *J. Am. Chem. Soc.*, 2004, **126**, 8380–8381.
24 V. M. Guerin and T. Pauporte, *Energy Environ. Sci.*, 2011, **4**, 2971–2979.
25 F. Shao, J. Sun, L. Gao, S. W. Yang and J. Q. Luo, *ACS Appl. Mater. Interfaces*, 2011, **3**, 2148–2153.
26 F. W. Zhuge, J. J. Qiu, X. M. Li, X. D. Gao, X. Y. Gan and W. D. Yu, *Adv. Mater.*, 2011, **23**, 1330–1334.
27 J. Qu, G. R. Li and X. P. Gao, *Energy Environ. Sci.*, 2010, **3**, 2003–2009.
28 Q. Wang, J. E. Moser and M. Gratzel, *J. Phys. Chem. B*, 2005, **109**, 14945–14953.
29 J. K. Chen, K. X. Li, Y. H. Luo, X. Z. Guo, D. M. Li, M. H. Deng, S. Q. Huang and Q. B. Meng, *Carbon*, 2009, **47**, 2704–2708.
30 S. Baik, Q. Zheng, H. Kang, J. Yun, J. Lee and J. H. Park, *ACS Nano*, 2011, **5**, 5088–5093.
31 T. Y. Peng, K. Fan, W. Zhang, J. N. Chen and F. Yang, *J. Phys. Chem. C*, 2011, **115**, 17213–17219.
32 S. R. Sun, L. Gao and Y. Q. Liu, *Appl. Phys. Lett.*, 2010, **96**, 083113.
33 F. Z. Huang, D. H. Chen, L. Cao, R. A. Caruso and Y. B. Cheng, *Energy Environ. Sci.*, 2011, **4**, 2803–2806.
34 L. L. Li, Y. J. Chen, H. P. Wu, N. S. Wang and E. W. G. Diau, *Energy Environ. Sci.*, 2011, **4**, 3420–3425.

Downloaded by University of Science and Technology of China on 18 October 2012
Published on 27 February 2012 on http://pubs.rsc.org | doi:10.1039/C2JM15442K

This journal is © The Royal Society of Chemistry 2012